Green and Smart Mining Engineering 1 (2024) 58–66

Contents lists available at ScienceDirect

Green and Smart Mining Engineering

journal homepage: www.keaipublishing.com/en/journals/gsme

Novel recovery of a low-concentration gold thiosulfate complex through electroreduction via a walnut shell charcoal electrode

Qizheng Weng[a,b], Shaoxian Song[a,b], Weiquan Zhan[a,b,c,*], Xuan Zhang[a,b], Ziwei Xiang[a,b], Jiabei Gao[a,b], Feifei Jia[a,b,*]

[a] Key Laboratory of Green Utilization of Critical Non-metallic Mineral Resources of Ministry of Education, Wuhan University of Technology, Wuhan 430070, China
[b] Hubei Key Laboratory of Mineral Resources Processing and Environment, Wuhan University of Technology, Wuhan 430070, China
[c] Instituto de Fisica, Universidad Autonoma de San Luis Potosi, Av. Manuel Nava 6, Zona Universitaria, C.P. 78290 San Luis Potosi, S.L.P., Mexico

ARTICLE INFO

Keywords:
Electroreduction
Low concentration
$Au(S_2O_3)_2^{3-}$
Au^0
Walnut shell charcoal electrode

ABSTRACT

Low-concentration $Au(S_2O_3)_2^{3-}$ recovery is an urgent issue to facilitate the application of thiosulfate leaching instead of cyanide leaching in factories. Herein, this work presents a novel recovery of low-concentration $Au(S_2O_3)_2^{3-}$ combining adsorption and electrodeposition (electroreduction) to realize high $Au(S_2O_3)_2^{3-}$ recovery in the form of gold particles (Au^0). Walnut shells were used as the raw material for the successful preparation of charcoal with porous structure and rich oxygen-containing functional groups. Walnut shell charcoal (WSC) as the electrode achieved efficient recovery of low-concentration $Au(S_2O_3)_2^{3-}$. The recovery under low-concentration conditions was higher than 90%, with the highest reduction of 46.97 $mg \cdot g^{-1}$. Applying a suitable low voltage (0.8 V) facilitated low-concentration $Au(S_2O_3)_2^{3-}$ recovery, which was immensely improved than that without voltage. $Au(S_2O_3)_2^{3-}$ recovery performances under applied voltage via the WSC electrode were related to electrochemical abilities, including reaction intensity and charge transfer. More reactive sites containing suitable pores and oxygen functional groups were beneficial for the reduction reaction. This work offers a new way to recover low-concentration $Au(S_2O_3)_2^{3-}$ via cheap charcoal electrodes from solutions for application in the cyanide-free leaching method in industry.

1. Introduction

As a valuable metal, gold has wide applications with enormous significance in the economy [1], industry [2], science [3], and culture [4]. Cyanide leaching is a well-established method for extracting gold from ores [5,6], which occupies a dominant position in industry [7]. Over time, there has been an evolution in the processes used for extracting gold as the world develops [8,9], with a focus on economic efficiency and environmental sustainability [10,11]. With the continuous exploitation of rich gold ores, most existing gold deposits have low-grade characteristics [12]. The classical cyanide leaching method hardly extracts refractory ore, such as gold ore containing carbon [13]. Moreover, this strategy has other drawbacks, such as high toxicity [14] and high energy consumption [15], which would damage the environment [16]. Thus, developing an alternative to cyanide leaching for actual applications is urgently needed.

Thiosulfate leaching is one of the most promising methods for industrial applications among cyanide-free leaching methods, including the halogen leaching method [17], thiourea leaching method [18,19], and thiocyanate leaching method [20,21]. Due to its environmental friendliness and great selectivity in gold extraction [22–24], thiosulfate is an effective complexing agent that enhances the solubility and recovery of metals because of its high selectivity and ability to resist interference from impurity ions; thus, it has potential in leaching gold mines with low-grade characteristics, especially gold ores containing carbon [25,26]. Moreover, because of the inorganic salt property of thiosulfate, the environmental impact of using thiosulfate leaching is minimal [27,28]. Nevertheless, the application of the thiosulfate leaching method for low-concentration gold thiosulfate complex ($Au(S_2O_3)_2^{3-}$) recovery from leaching solutions is difficult.

Currently, methods for $Au(S_2O_3)_2^{3-}$ recovery from leaching solutions are precipitation [29], solvent extraction [30], adsorption [31],

Peer review under the responsibility of Editorial Board of Green and Smart Mining Engineering.
* Corresponding authors at: Key Laboratory of Green Utilization of Critical Non-metallic Mineral Resources of Ministry of Education, Wuhan University of Technology, Wuhan 430070, China.
E-mail addresses: zhan_weiquan@163.com (W. Zhan), feifeijia@whut.edu.cn (F. Jia).

https://doi.org/10.1016/j.gsme.2024.03.004
Received 29 December 2023; Received in revised form 28 February 2024; Accepted 5 March 2024
Available online 22 March 2024

and electrodeposition [32]. The product obtained via the displacement precipitation process contains impurities and has a low grade. Solvent extraction is an expensive process that requires a significant number of organic solvents and strict control over the reaction conditions, resulting in increased manufacturing costs [33]. The adsorption method is a simple and cost-effective technique that facilitates the interaction between ions and materials [34]. However, the process of adsorption may encounter issues such as inadequate or excessive adsorption, which can lead to a reduction in the amount of recovered gold [35]. The electrodeposition method allows the migration and reduction of ions in solution, but the recovery of $Au(S_2O_3)_2^{3-}$, particularly at low concentrations, is inadequate [36], possibly owing to insufficient force.

Considering that enhanced interaction between electrode and Au $(S_2O_3)_2^{3-}$ could be improved through applying materials, combining the advantages of adsorption and electrodeposition could be adopted for realizing efficient recovery of $Au(S_2O_3)_2^{3-}$ as well as reduction [37,38]. When the material is introduced, the attractive force between targeted ions and material would be greatly enhanced [39], thus strengthening the migration of $Au(S_2O_3)_2^{3-}$ in solutions and the reaction of $Au(S_2O_3)_2^{3-}$ on the electrode. Electroreduction is achieved by coating materials on traditional titanium (Ti) plates to recover low-concentration $Au(S_2O_3)_2^{3-}$ from aqueous solutions. The electroreduction method has been applied in metal ion recovery [40], such as Cr(VI) [41], Bi(III) [42], and Zn(II) [43], achieving simultaneous recovery and reduction. Herein, this approach could solve the problem of low-concentration $Au(S_2O_3)_2^{3-}$ recovery.

Charcoal has the merits of a large specific surface area and rich oxygen-containing functional groups, which provide sufficient reactive sites with $Au(S_2O_3)_2^{3-}$ [44,45]. Walnut shells could be converted into biochar with high adsorption properties through a specific preparation process [46]. They are widely available and cost-effective, providing a rich source of raw materials for biochar production, especially in China [47]. Walnut shell charcoal (WSC) has been proven that it can be utilized not only for adsorbing metal ions but also as a catalyst carrier or electrode material [48]. A titanium (Ti) plate with high conductivity [49] and good stability [50] can be applied as the substrate for coating charcoal materials to prepare the electrodes. In this work, electroreduction using the WSC electrode is proposed to achieve simultaneous efficient recovery of low-concentration $Au(S_2O_3)_2^{3-}$ and reduction.

2. Experimental

2.1. Materials

Walnuts were bought from Zhiyin Store, Wuhan Province, China. Standard chloroauric acid ($HAuCl_4$, 1000 mg·L^{-1}) was purchased from Well Group Scientific Ltd., USA. Ammonium thiosulfate (98wt%) was obtained from Sigma-Aldrich (Shanghai, China). Sodium hydroxide (NaOH), Na_2SO_4, and dimethylacetamide (DMA) (12.5 mg·mL^{-1}) were obtained from Sinopharm Chemical Reagent Co., Ltd. (Shanghai, China). Vinylidene fluoride was procured from Alfa Aesar (China) Chemicals Co., Ltd. Conductive carbon black was obtained from American Cabot, while carbon black was acquired from Suzhou Sinero Technology Co., Ltd. (China). Deionized water was produced by Millipore SAS (France) with 18.2 MΩ·cm.

2.2. Preparation of the WSC electrode

Walnut shells were crushed into powder using a crusher and screened with a 200-mesh sieve (about 0.075 mm) as the original materials. Then, the powder was placed in a porcelain boat and heated in a tube furnace at certain carbonization temperatures (400, 500, 600, 700, and 800 °C) in a nitrogen atmosphere for 60 min. After cooling down to room temperature, the obtained black samples were washed with ethanol and deionized water with mass ratios of deionized water and ethanol to samples of about 1:900 and 1:100, respectively, to purify the product. Through freeze-drying at − 20 °C in vacuum, the WSC was finally obtained. WSC is denoted as WSC-X, where X is the carbonization temperature.

WSC, conductive carbon black, and polyvinylidene fluoride were mixed evenly at a mass ratio of 8:1:1 in a mortar and dissolved in DMA. Then, with approximately 30 ± 5 mg of the mixture, using the flat part on the back of the spoon, it was evenly coated on the Ti plate. Next, the electrode was heated at 60 °C for at least 1 h to remove the residual organic solvent. Finally, the prepared electrode was immersed in deionized water to form and dried before use.

2.3. $Au(S_2O_3)_2^{3-}$ recovery by electroreduction

Briefly, a certain molar ratio (Au to $S_2O_3^{2-}$ as 1 to 4) of ammonium thiosulfate was mixed with deionized water, and an appropriate amount of sodium hydroxide was added to control the pH to 10. Afterward, chloroauric acid and sodium hydroxide were added dropwise in turn. During the process, the pH of the solution should be maintained at 10. After all the required chloroauric acid had been added, the volume of the solution was adjusted to 200 mL.

Two electrodes coated with WSC with a specific voltage were put at a certain distance into the electrolytic cell that contained the solution (Fig. S1). The electrolytic cell was connected to a peristaltic pump, and the solution was cycled at a speed of 50 r/min. At a certain time, 2.5 mL of solution was extracted and filtered using a 0.22 μm filter membrane. The concentration of filtrate was determined using an atomic absorption spectrometer. The following formulas were used to calculate the reduction capacity (Q) and recovery (R):

$$Q = \frac{(C_0 - C_t) \times (V_0 - V_t)}{m} \quad (1)$$

$$R = \frac{(C_0 - C_t)}{C_0} \times 100\% \quad (2)$$

where C_0 and C_t are the concentrations of Au at the initial and time t, respectively, mg·L^{-1}; V_0 and V_t are the volumes of reaction solution at the initial and time t, respectively, L; m is the material mass used in the electrode, mg.

2.4. Characterizations

The pyrolysis of walnut shell powder was analyzed using a synchronous thermal analyzer (Nechi, STA449F3Jupiter, Germany) in a high-purity nitrogen atmosphere at a heating rate of 10 °C·min^{-1} from room temperature to 800 °C. The internal structure and morphology of materials were analyzed by X-ray diffraction (XRD, D8 Advance, Bruker AXS, Germany) using Cu-K_α radiation. Raman spectra were collected using an INVIA Raman microscope with an Ar laser (Renishaw, England). Surface functional groups were analyzed using an American Nexus Fourier transform infrared spectrometer in the wavenumber range of 4000–400 cm^{-1}. Pore structure distribution, adsorption and desorption isotherms were studied by the Brunauer–Emmett–Teller method (BET, V-Sorb X800, China). Microstructures and corresponding energy dispersive spectra (EDS) were collected on a scanning electron microscope (SEM, Phenom ProX G6, Netherlands) and transmission electron microscope (TEM, FEI Tecnai G2 F20, America). The chemical element state was determined by X-ray photoelectron spectroscopy (XPS, Thermo Scientific K-Alpha, America). The gold concentration of the solution was determined using an Agilent 280FS AA Spectrometer (G8434A, America).

2.5. Electrochemical measurements

Cyclic voltammetry (CV) and electrochemical impedance spectroscopy (EIS) were applied. Both experiments were measured in 50 mL of 1 mol·L^{-1} Na_2SO_4 and 5 mg·L^{-1} $Au(S_2O_3)_2^{3-}$ via a three-electrode system (VersaSTAT-450, PAR, USA). The working electrode operated in

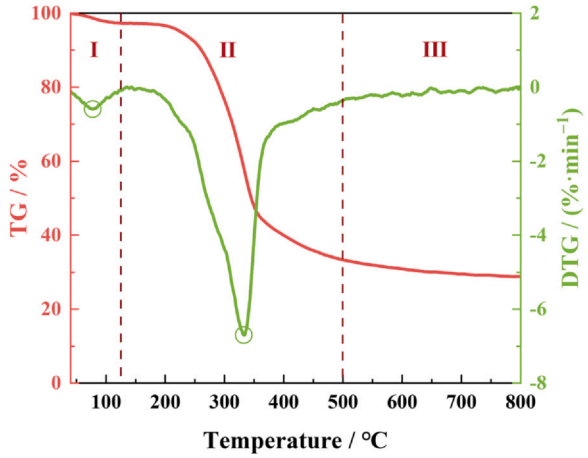

Fig. 1. TG spectra of walnut shell powder.

this experiment with about 1 cm^2 was made of the same material as the electrode in the Au removal process. A Pt plate and a Hg/HgO 1 M KOH electrode were the counter electrode and reference electrode, respectively. The frequency range of the EIS test was 0.01–10000 Hz.

3. Results and discussion

3.1. Synthesis of WSC

WSC was obtained from walnut shells by the carbonization method, and it could be divided into three stages according to the thermogravimetry (TG) analysis (Fig. 1). The first stage was the dehydration drying stage in the temperature range of 40–120 °C. Free water and molecular-bound water on the surface and inside of the sample were removed [51], and the mass loss was 2.64%. The second stage was pyrolysis in the temperature range of 120–500 °C. During the process at this temperature range, at first, the TG curve was almost linear, with only a small amount of mass loss (0.35%) due to the depolymerization reaction. Afterward, the TG curve decreased sharply, and most of the weight loss (63.71%) of the samples occurred in pyrolysis of cellulose and hemicellulose. Small molecular gases (such as CO, CO_2, and CH_4) and condensable macromolecule volatiles [52] were produced to generate pores. Meanwhile, an obvious weight loss peak could be seen in the corresponding differential thermogravimetry (DTG) analysis curve, and the weight loss rate reached the maximum at 333.3 °C, that is, the peak of the DTG curve, which was a main weight loss stage. The third stage was the slow decomposition stage of the residue in the temperature range of 500–800 °C. The weight loss ratio was 4.49%, and the weight loss process was relatively slow, mainly by lignin pyrolysis. At this time, the change of the DTG curve was slow, and the decomposition rate was slow [53–55]. Here, the WSC samples with various carbonization temperatures, from 400 to 800 °C, were synthesized to investigate the effect of carbonization temperature on electroreduction $Au(S_2O_3)_2^{3-}$ performances. According to the below equation, the yield (Y) was calculated.

$$Y = \frac{M_{bc}}{M_{bs}} \times 100\% \tag{3}$$

where M_{bc} and M_{bs} are the quality of biochar after and before pyrolysis, respectively, and Y is the yield. The final yield is 28.8%.

In all carbonization processes, different gases were produced, causing the pore size to increase with temperature and gradually reach saturation in the third stage.

3.2. Structure characterization

XRD, XPS, Raman, and FTIR were used to characterize the microstructure of WSC. There were two clear broad peaks at about 22° and 44° in Fig. 2(a), corresponding to the diffraction peaks of graphite carbon, which indicate that WSC belongs to typical amorphous carbon [56]. Upward warping at a low diffraction angle in WSC was ascribed to high porosity. A wide diffraction peak from 15° to 30° originated from the so-called graphite structure (002) crystal plane. The intensity of the (002) crystal plane diffraction peak was weaker, and the width was wider at the same time, which means that the graphitization degree of

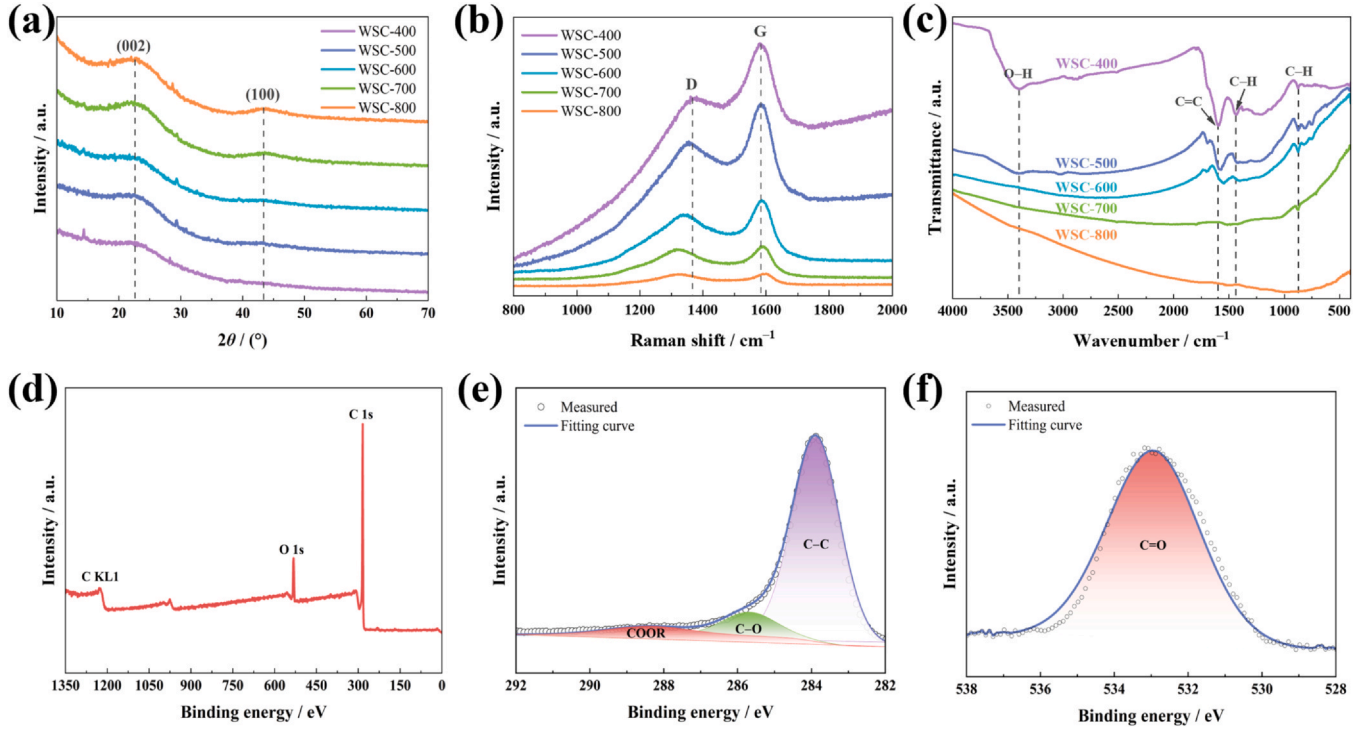

Fig. 2. (a) XRD patterns, (b) Raman patterns, (c) FTIR spectra, and XPS of WSC: (d) survey spectra, (e) C 1s spectra, and (f) O 1s spectra.

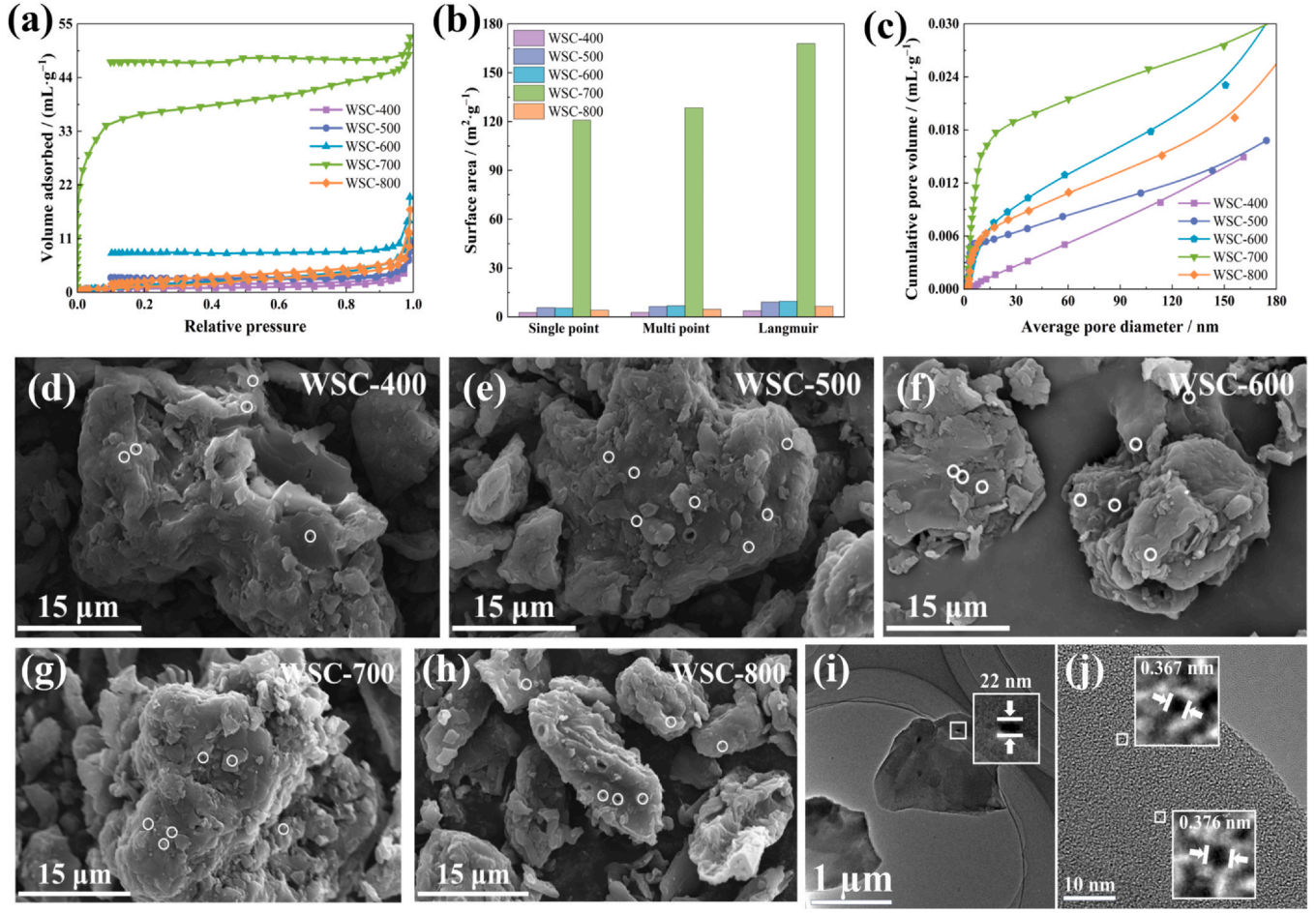

Fig. 3. (a) Nitrogen adsorption–desorption isotherms, (b) specific surface area, and (c) cumulative pore volume curves. SEM images of (d) WSC-400, (e) WSC-500, (f) WSC-600, (g) WSC-700, (h) WSC-800, and (i, j) TEM and HRTEM images of WSC.

WSC is relatively low. Moreover, the graphitization degree and order degree of WSC increased with the increase in carbonization temperature [57,58].

XPS was performed to investigate the chemical states of elements in WSC. There were strong absorption peaks at binding energies of 1223.89, 532.14, and 284.26 eV in the survey spectrum (Fig. 2(d)), belonging to the absorption peaks of C KL1, O 1s, and C 1s, respectively, which indicates that WSC is mainly composed of C and O elements. Fig. 2(e) shows the C 1s XPS spectrum of WSC, revealing the carbon atoms of three groups on the surface. Binding energy peaks at 283.88, 285.68, and 288.38 eV corresponded to the C–C, C–O, and COOR, respectively [59]. Fig. 2(f) shows the O 1s XPS spectrum of WSC, and the binding energy peak at 532.03 eV was a typical O 1s absorption peak.

The molecular vibration and rotation of functional groups of WSC were tested by Raman (Fig. 2(b)). The characteristic peak at 1361 cm^{-1} originated from the vibration of the graphite carbon crystal edge, called the D band, representing the defect of the C atomic lattice. The characteristic peak at 1580 cm^{-1} was a typical Raman peak of bulk crystalline graphite, called the G-band, representing the in-plane stretching vibration of the C atom sp^2 hybrid and the degree of carbonization of the material. This peak is the basic vibration mode of the graphite crystal, and its intensity is related to crystal size.

With the aim of further investigating more functional groups and their content in WSC, FTIR tests were performed, and the results are shown in Fig. 2(c). The peaks at 3405, 3100–2900, 2500, 1800–1700, 1600–1550, 1440–1400, 890–880, 825, and 761 cm^{-1} were attributed to the stretching vibration of O–H and stretching vibration of O–H, O–H, O–H, C–H, C═C, O–H, C–O, C–H, C–H, respectively [53,60]. The graph showed that with enhanced carbonization temperature, oxygen-containing functional groups of WSC gradually reduced. WSC-700 had fewer oxygen-containing functional groups, while none in WSC-800. The degree of graphitization of WSC increased in proportion to the decrease in oxygen-containing functional groups. These polar functional groups can improve the chemical interaction of WSC with Au $(S_2O_3)_2^{3-}$ as an electrode material.

3.3. Morphology and pore characteristics

The morphology of all WSC samples was characterized by SEM and TEM. In Fig. 3(d–h), all WSC samples had similar blocky morphology but various pores. In Fig. 3(d–j), it could be seen that all WSC possessed irregular holes, as revealed in white circles, corresponding to the results of cumulative pore volume curves. As the carbonization temperature increased, the amounts of pores increased while the size of the WSC decreased, which may be due to the gradual pyrolysis of lignin. Overall, the higher the carbonization temperature, the richer the pore size. In addition, the distorted areas of high-resolution transmission electron microscope (HRTEM) in Fig. 3(j) resulted from amorphous carbon. Pore characteristics were explored using the BET method. The N_2 adsorption–desorption curves of WSC in Fig. 3(a) belonged to the type IV curve, and there were adsorption hysteresis loops in the middle, corresponding to the capillary condensation system of porous adsorbents. The adsorption hysteresis ring was an H4 type of hysteresis ring, and the isotherm had no obvious saturated adsorption platform, indicating that the pore structure of the prepared WSC is very irregular. Based on the curves, the specific surface areas of the WSC samples are given in

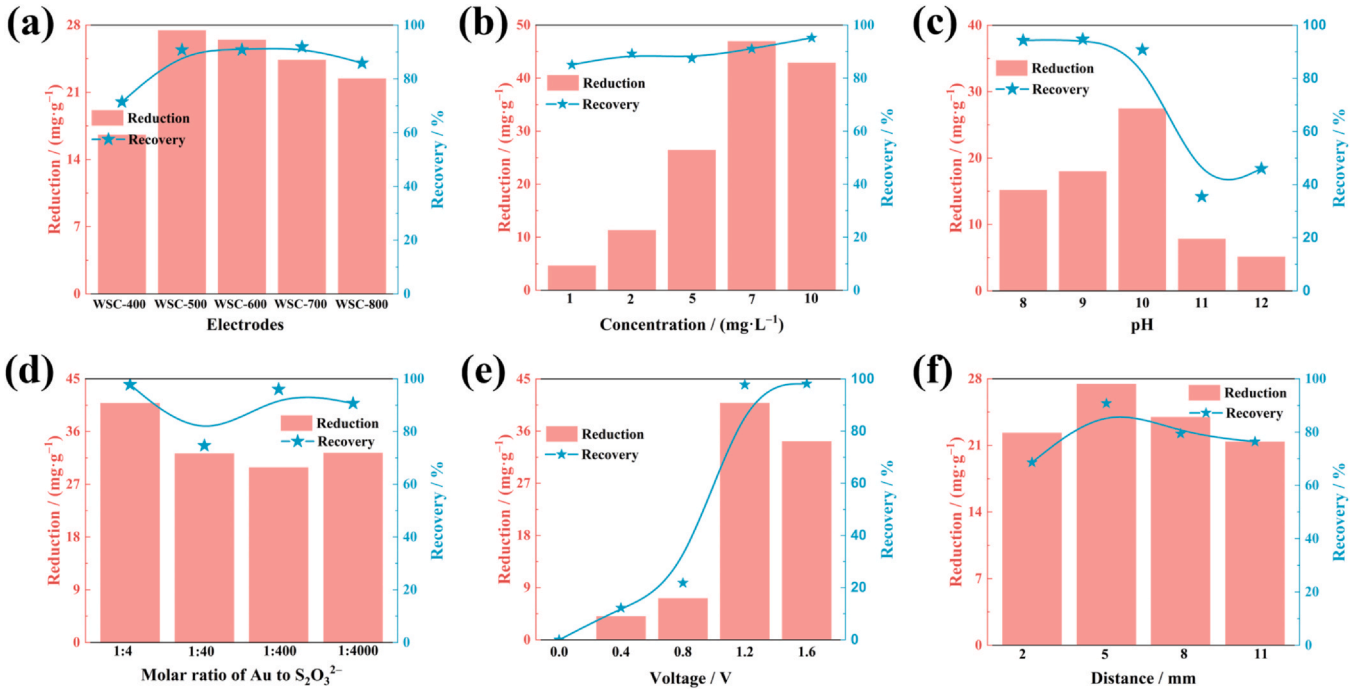

Fig. 4. $Au(S_2O_3)_2^{3-}$ recovery performance under different environmental conditions: (a) material, (b) concentration, (c) pH, (d) molar ratio of Au to $S_2O_3^{2-}$, (e) applied voltage, and (f) distance between two electrodes.

Table 1
Comparison of the recovery capacities of WSC and other materials.

Material	Concentration (mg/g)	Recovery capacity (mg/g)	Recovery (%)	References
Cupric ferrocyanide-impregnated activated carbon	100	1.474	75	[64]
Silver ferrocyanide-impregnated activated carbon	100	1.212	70	[65]
1-methyl-5-mercapto-1,2,3,4-tetrazole-impregnated activated carbon	10	1.9	94	[66]
Thiocyanate-activated activated carbon	150	11.86	79	[67]
Walnut shells charcoal	10	42.9	95	This work

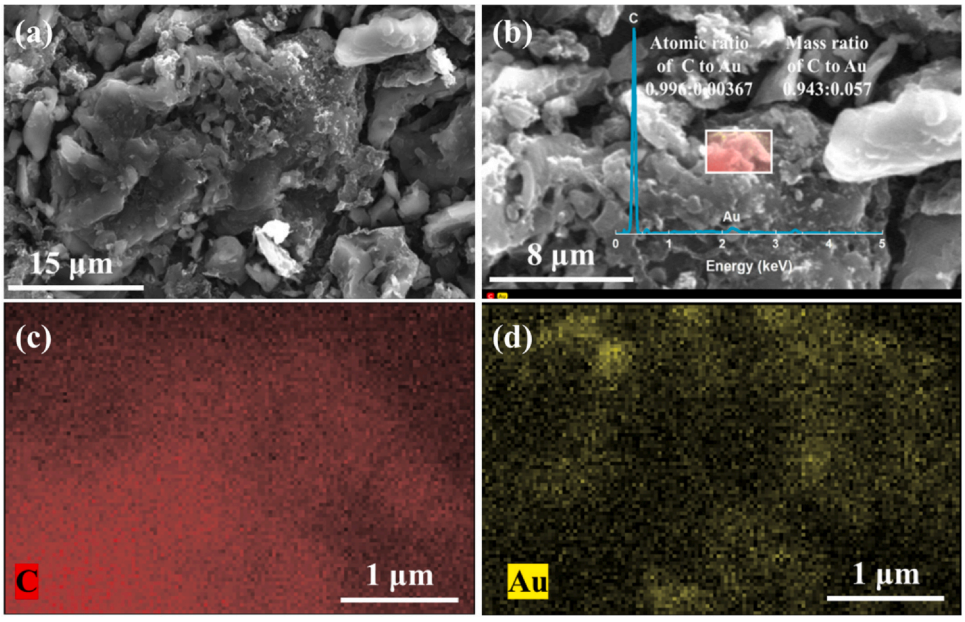

Fig. 5. (a, b) SEM images and EDS elemental distribution mapping of (c) C and (d) Au patterns of the WSC electrode after $Au(S_2O_3)_2^{3-}$ recovery.

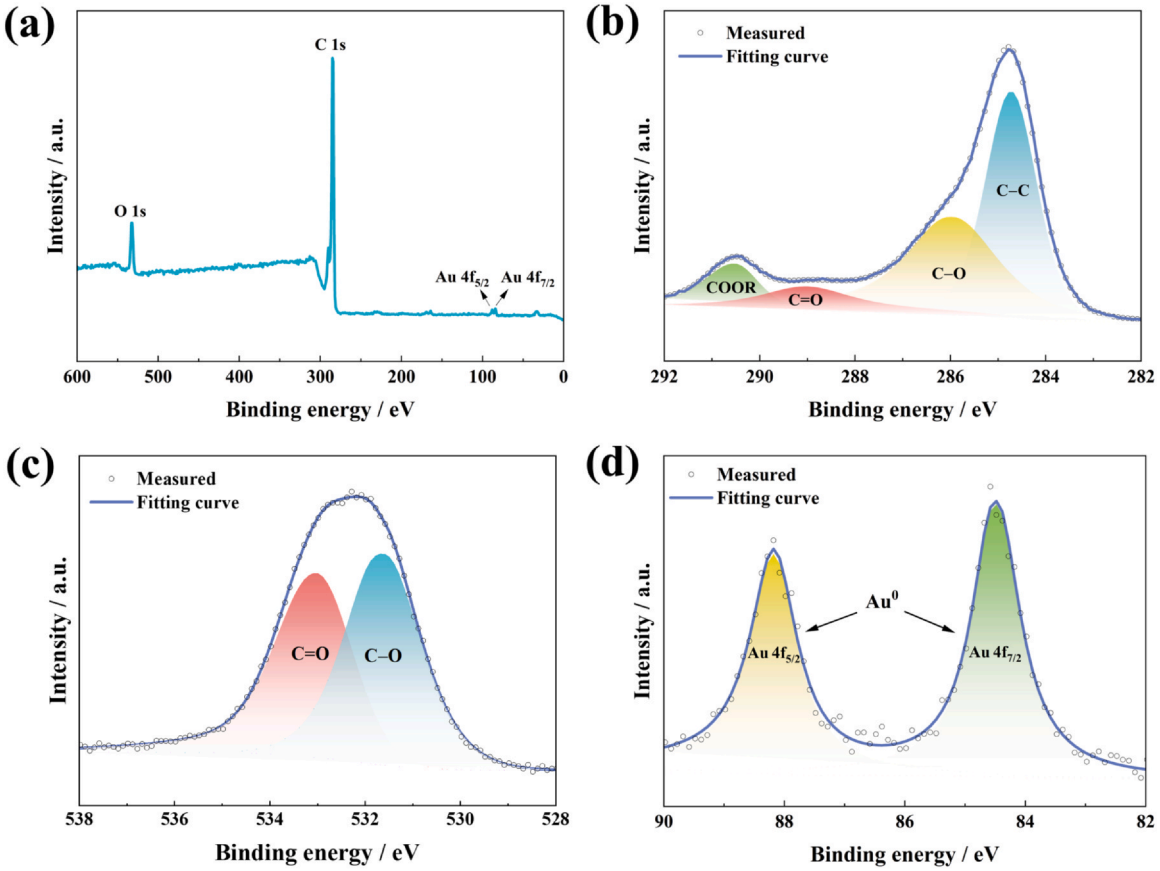

Fig. 6. (a) XPS survey spectra, (b) C 1s XPS spectra, (c) O 1s XPS spectra, and (d) Au 4f spectra of the WSC electrode after $Au(S_2O_3)_2^{3-}$ recovery.

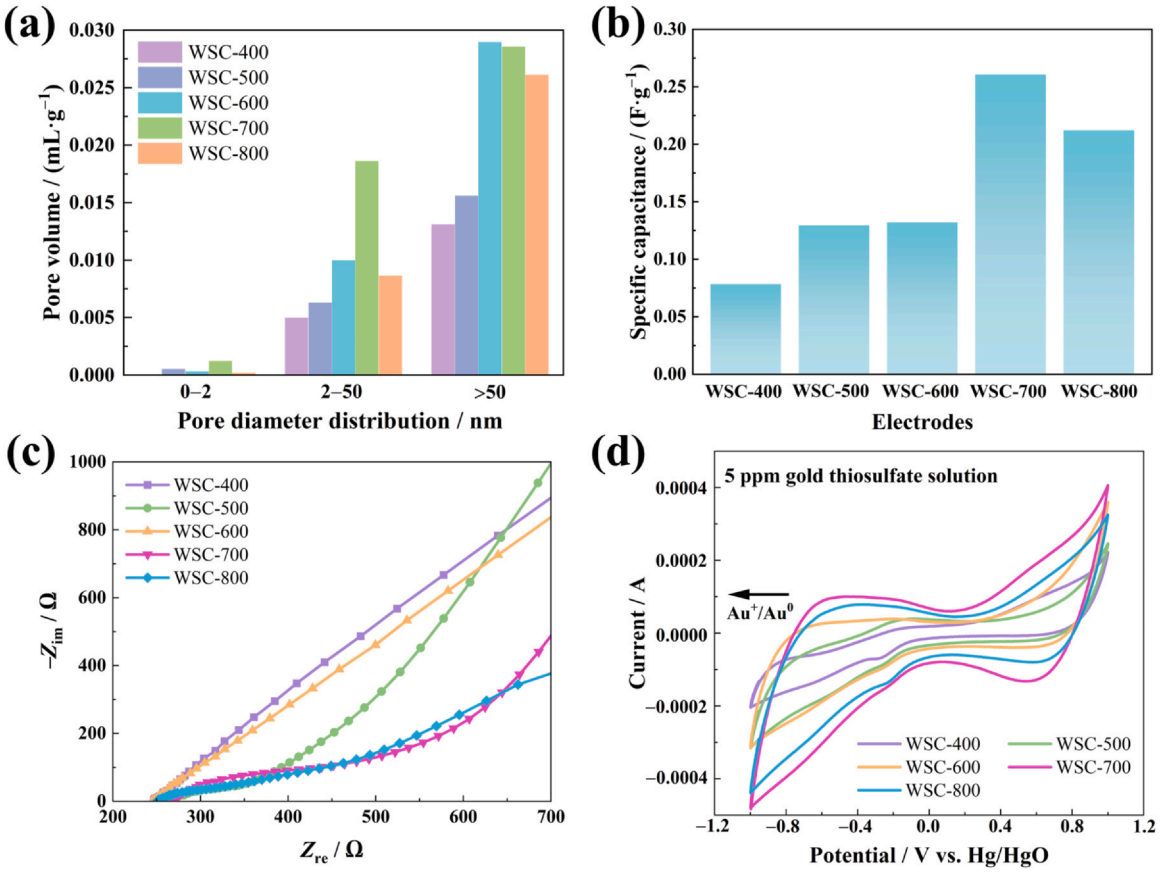

Fig. 7. (a) Pore diameter distributions of WSC, (b) specific capacitances of WSC in $Au(S_2O_3)_2^{3-}$ solutions, (c) EIS curves, and (d) CV curves scanned at 1 $mV \cdot s^{-1}$.

Fig. 3(b). The specific surface area increased with the increase in carbonization temperature, reached the maximum at a certain carbonization temperature, and then decreased. A large surface area is beneficial for providing more active sites. Furthermore, the pore structure of WSC was obtained, and the cumulative pore volume curves are shown in Fig. 3(c). It can be concluded that there were more pores when increasing the carbonization temperature. At higher than 700 °C, the pore channel collapsed, resulting in decreased pores and specific surface areas.

3.4. $Au(S_2O_3)_2^{3-}$ recovery performances by electroreduction

$Au(S_2O_3)_2^{3-}$ recovery performances by the WSC electrode under various environmental conditions were evaluated. Fig. 4(a) shows the adsorption capacity and corresponding recovery of different WSC electrodes. WSC electrodes showed excellent recovery of $Au(S_2O_3)_2^{3-}$ (highest recovery of 95%), with WSC-400 having the lowest adsorption capacity. With the increase in carbonatization temperature, recovery improved and then plateaued after dropping a little. The dropped recovery, as observed for the WSC-800 electrode, may originate from a less functional group and a corresponding smaller electric double layer for ion storage. Recovery performances under different solution concentrations (1, 2, 5, 7, and 10 $mg{\cdot}L^{-1}$) are depicted in Fig. 4(b). Within the solution concentration range of 1–10 $mg{\cdot}L^{-1}$, the WSC electrode exhibited excellent recovery and adsorption capacity of $Au(S_2O_3)_2^{3-}$, confirming that low-concentration Au $(S_2O_3)_2^{3-}$ can be efficiently recovered by electroreduction.

Furthermore, solution environmental and operating parameters such as pH, applied voltage, distance between electrodes, and molar ratio of Au to $S_2O_3^{2-}$ were considered. Because $Au(S_2O_3)_2^{3-}$ is stable in alkaline conditions, the solution pH from 8 to 12 was examined (Fig. 4(c)). It was obvious that the recovery maintained a high value until 10 and then dropped due to the increase in competitive ion OH^- for reactive sites [61]. Applied voltage was a key parameter during $Au(S_2O_3)_2^{3-}$ recovery (Fig. 4(e)). When no voltage was applied, the recovery performance of $Au(S_2O_3)_2^{3-}$ was very poor. After applying voltage on the electrode, Au $(S_2O_3)_2^{3-}$ immigrated in solution, and recovery increased with the increase in voltage. The reduction and recovery at 0.8 V were greatly improved than those without voltage, respectively. The recovery greatly changed with applied voltages of 1.2 and 0.8 V, perhaps due to the electrostatic interactions between ions and porous electrodes becoming stronger as the voltage increased. These interactions tended to induce ions into the pores. When the voltage increased sufficiently high, the influence of electrostatic interactions overcame that of volume repulsion interactions, and ions began to accumulate in the pores. As ions accumulated in the pores, they induced surface charges on the porous electrode. These enhanced surface charges attracted more ions to enter the pores [62]. Compared with recovery at 0.8 V, recovery at 1.2 V may have reached the stage where the influence of electrostatic interaction overcame that of volume repulsion interaction. Fig. 4(f) illustrates the reduction performances at different plate spacings, showing a trend of first increasing and then decreasing reduction and recovery. It was inferred that when the distance between the plates is very close, the solution convection between two electrodes is reduced, resulting in decreasing recovery [63]. Meanwhile, when the distance between the plates is very far, the effect of the electric field force on recovering gold is weakened. In fact, in the application of thiosulfate leaching, $S_2O_3^{2-}$ was added excessively, so experiments with different molar ratios of gold and thiosulfate were also performed. As shown in Fig. 4(d), reduction and recovery were not affected significantly, which indicates a great potential application in thiosulfate leaching solutions. Compared with other works using similar materials in Table 1, this work achieved efficient and high recovery of $Au(S_2O_3)_2^{3-}$.

During the recovery process, a small portion of the material dropped off from the electrode plate, accounting for approximately 2%–4% mass loss. Compared with the total mass, the lost materials made up only a small portion.

3.5. Gold element state after $Au(S_2O_3)_2^{3-}$ recovery

After being applied as an electrode for $Au(S_2O_3)_2^{3-}$ electroreduction, the gold state on WSC was explored by SEM–EDS and XPS. The SEM images (Fig. 5(a)) showed a similar morphology to before, with the corresponding EDS elemental distribution (Fig. 5(b)). Fig. 5(d) indicates the good distribution of Au on the surface of the WSC electrode. Furthermore, XPS was conducted to study the gold element state and interaction. From the XPS survey spectrum, Au and C elements were observed on the WSC electrode after $Au(S_2O_3)_2^{3-}$ recovery, confirming the successful gold recovery experiment. To further study the state of the gold, the Au 4f XPS spectrum was collected and is displayed in Fig. 6(d). The binding energy peaks at 84.4 and 88.0 eV were associated with the Au $4f_{7/2}$ and Au $4f_{5/2}$ peaks, respectively, indicating the presence of the gold element (Au^0) after the recovery experiment. As for the other element spectra, such as C and O, they showed the same functional groups as before recovery. The above results demonstrated that $Au(S_2O_3)_2^{3-}$ was successfully recovered in the form of gold particles by the WSC electrode.

3.6. Electrochemical behaviors of WSC electrodes

To explore the electrochemical behaviors of WSC, CV and EIS were conducted in Na_2SO_4 (Figs. S2 and S3) and $Au(S_2O_3)_2^{3-}$ (Fig. 7(c, d)) solutions. As shown in Fig. S3, the electrodes displayed a good rectangular shape without obvious redox peaks, suggesting that the capacitance is mainly provided by the electric double layer. All WSC samples showed similar ion storage ability. According to calculations in Fig. S4, WSC-500 had the highest specific capacitance. To further investigate the reaction process, the CV curve revealed that in Au $(S_2O_3)_2^{3-}$ solution (Fig. 7(d)), gold depletion occurred in the range of − 0.2 to − 0.8 V, demonstrating a reduction reaction. The area under the CV curve first increased and then decreased, with WSC-700 having the highest capacitance, which was beneficial for the reaction of Au $(S_2O_3)_2^{3-}$. The recovery performances would be related to mesoporous structure (Fig. 7(a)) because they usually served as the reactive sites. The better recoveries of WSC-500 and WSC-600 than WSC-800 were due to more oxygen functional groups interacting with $Au(S_2O_3)_2^{3-}$. The EIS curves in $Au(S_2O_3)_2^{3-}$ (Fig. 7(c)) and Na_2SO_4 (Fig. S2) showed a small semicircle arc, with WSC-400 showing the largest impedance. With lower charge transfer and reactive sites, WSC-400 had the poorest recovery ability of $Au(S_2O_3)_2^{3-}$. Therefore, the $Au(S_2O_3)_2^{3-}$ recovery ability depends on both reaction ability and charge transfer.

4. Conclusion

The biochar electrode based on WSC was successfully prepared to achieve the efficient recovery of gold at low concentrations. For an initial concentration range of 1–10 $mg{\cdot}L^{-1}$, the recovery rate for gold was over 85%, with the highest recovery of 95%, corresponding to a reduction of 42.9 $mg{\cdot}g^{-1}$. Walnut shells were used as the raw material for the successful preparation of WSC with a good pore structure and a rich content of oxygen-containing functional groups. WSC was then used as the electrode material for the efficient reduction and recovery of low-concentration $Au(S_2O_3)_2^{3-}$ by electroreduction methods. This has great potential in low-concentration $Au(S_2O_3)_2^{3-}$ recovery. The recovery performance of $Au(S_2O_3)_2^{3-}$ in the electroreduction method was linked to the pore size and number of functional groups of the electrode material. The greater the number of functional groups and pore size active sites, the better the recovery effect. Applying a suitable low voltage was an efficient method for the recovery of $Au(S_2O_3)_2^{3-}$, with low power, low energy consumption, environmental friendliness, and a simple process. This work offers new insights into the electrochemical recovery of low-concentration gold elements from solutions by electroreduction.

CRediT authorship contribution statement

Qizheng Weng: Conceptualization, Data curation, Formal analysis, Writing – original draft. **Shaoxian Song:** Formal analysis, Edit – review & editing. **Weiquan Zhan:** Formal analysis, Data curation, Edit – original draft. **Xuan Zhang:** Software, Investigation. **Ziwei Xiang:** Modification. **Jiabei Gao:** Equipment support. **Feifei Jia:** Edit – review & editing.

Declaration of Competing Interest

Shaoxian Song is an editorial board member for this journal and was not involved in the editorial review or the decision to publish this article. The authors declare that they have no known competing financial interests or personal relationships that could have appeared to influence the work reported in this paper.

Acknowledgements

This work was financially supported by the National Key Research and Development Program of China (No. 2021YFC2900900). Dr. Zhan gratefully acknowledges the Consejo Nacional de Humanidades Ciencias y Tecnologías (CONAHCYT) of Mexico for offering him the scholarship under the grant No. 813934 during his Ph.D. studies.

Appendix A. Supporting information

Supplementary data associated with this article can be found in the online version at doi:10.1016/j.gsme.2024.03.004.

References

[1] C. Wang, G. Lin, J.L. Zhao, S.X. Wang, L.B. Zhang, Y.H. Xi, X.T. Li, Y. Ying, Highly selective recovery of Au(III) from wastewater by thioctic acid modified Zr-MOF: experiment and DFT calculation, Chem. Eng. J. 380 (2020) 122511.
[2] Z. Lu, T. Li, S.R. Mudshinge, B. Xu, G.B. Hammond, Optimization of catalysts and conditions in gold(I) catalysis-counterion and additive effects, Chem. Rev. 121 (14) (2021) 8452–8477.
[3] S. Choi, S.I. Han, D. Jung, H.J. Hwang, C. Lim, S. Bae, O.K. Park, C.M. Tschabrunn, M. Lee, S.Y. Bae, J.W. Yu, J.H. Ryu, S.W. Lee, K. Park, P.M. Kang, W.B. Lee, R. Nezafat, T. Hyeon, D.H. Kim, Highly conductive, stretchable and biocompatible Ag–Au core–sheath nanowire composite for wearable and implantable bioelectronics, Nat. Nanotechnol. 13 (2018) 1048–1056.
[4] H.L. Qian, F.L. Meng, C.X. Yang, X.P. Yan, Irreversible amide-linked covalent organic framework for selective and ultrafast gold recovery, Angew. Chem. Int. Ed Engl. 59 (40) (2020) 17607–17613.
[5] X.E. Dang, W.S. Ke, C. Tang, J. Lv, X. Zhou, C.P. Liu, Increasing leaching rate of gold cyanide of two-stage calcination generated from refractory ore containing arsenopyrite and pyrrhotite, Rare Met 35 (10) (2016) 804–810.
[6] J.S. Xia, R. Marthi, J. Twinney, A. Ghahreman, A review on adsorption mechanism of gold cyanide complex onto activation carbon, J. Ind. Eng. Chem 111 (2022) 35–42.
[7] H.Q. Niu, H.Y. Yang, L.L. Tong, Research on gold leaching of carbonaceous pressure-oxidized gold ore via a highly effective, green and low toxic agent trichloroisocyanuric acid, J. Clean. Prod 419 (2023) 138062.
[8] S.S. Konyratbekova, A. Baikonurova, A. Akcil, Non-cyanide leaching processes in gold hydrometallurgy and iodine-iodide applications: a review, Miner. Process. Extr. Metall. Rev. 36 (3) (2015) 198–212.
[9] C.B. Sun, X.L. Zhang, J. Kou, Y. Xing, A review of gold extraction using noncyanide lixiviants: Fundamentals, advancements, and challenges toward alkaline sulfur-containing leaching agents, Int. J. Miner. Metall. Mater. 27 (4) (2020) 417–431.
[10] L. Liao, Y.H. Song, P.P. Zhang, Y.F. Li, J. Bao, J.M. Zhou, Treatment of actual cyanide gold extraction wastewater by persulfate oxidation and its reaction mechanism, Res. Chem. Intermed. 49 (8) (2023) 3705–3721.
[11] S.J. Zhou, W.C. Li, W.G. Liu, J.B. Zhai, Removal of metal ions from cyanide gold extraction wastewater by alkaline ion-exchange fibers, Hydrometallurgy 215 (2023) 105992.
[12] I. Birloaga, I. De Michelis, F. Ferella, M. Buzatu, F. Vegliò, Study on the influence of various factors in the hydrometallurgical processing of waste printed circuit boards for copper and gold recovery, Waste Manag 33 (4) (2013) 935–941.
[13] Y.B. Yang, Z.H. Xie, B. Xu, Q. Li, T. Jiang, Gold extraction from a high carbon low-grade refractory gold ore by flotation–roasting–leaching process, in: N.R. Neelameggham, S. Alam, H. Oosterhof, A. Jha, D. Dreisinger, S. Wang (Eds.), Rare Metal Technology, 2015 Springer, Cham, 2015, pp. 63–70.
[14] L. Zhang, T. Jiang, X.Y. Guo, Q.H. Tian, S.P. Zhong, L. Dong, H. Qin, Z.W. Liu, B. Makuza, Sustainable processing of gold cyanide tailings: reduction roasting, mechanical activation, non-cyanide leaching, and magnetic separation, Hydrometallurgy 217 (2023) 106028.
[15] L. Jones, R.P. Hackl, Sources of high cyanide consumption for a biooxidized refractory gold concentrate, Process. Metall. 9 (C) (1999) 337–346.
[16] W.Q. Zhan, Y. Yuan, X. Yao, B.Q. Yang, F.F. Jia, C.S. Lin, J.L. Arauz-Lara, S.X. Song, Efficient recovery of gold(I) from thiosulfate solutions through photocatalytic reduction with Mn(II)-doped MoS_2, ACS Sustain. Chem. Eng 9 (35) (2021) 11681–11690.
[17] A. Filcenco Olteanu, T. Dobre, E. Panturu, A.D. Radu, A. Akcil, Experimental process analysis and mathematical modeling for selective gold leaching from slag through wet chlorination, Hydrometallurgy 144-145 (2014) 170–185.
[18] K. Li, Q. Li, Y. Zhang, X.L. Liu, Y.B. Yang, T. Jiang, Improved thiourea leaching of gold from a gold ore using additives, Hydrometallurgy 222 (2023) 106204.
[19] M.R. Ahmed, H.S. Mohammed, M.G. El-Feky, Y.K. Abdel-Monem, Gold leaching using thiourea from uranium tailing material, Gabal El-Missikat, Central Eastern Desert, Egypt, J. Sustain. Metall 6 (4) (2020) 599–611.
[20] G. Le, W.J. Li, K. Song, Y.S. Song, Y. Chen, A.P. Bai, Y. Cheng, Electrochemical dissolution behavior of gold and its main coexistent sulfide minerals in acid thiocyanate solutions, Rare Met 41 (1) (2022) 254–261.
[21] H. Wu, Y.L. Feng, W.F. Huang, H.R. Li, S.D. Liao, The role of glycine in the ammonium thiocyanate leaching of gold, Hydrometallurgy 185 (2019) 111–116.
[22] B. Xu, W.H. Kong, Q. Li, Y.B. Yang, T. Jiang, X.L. Liu, A review of thiosulfate leaching of gold: Focus on thiosulfate consumption and gold recovery from pregnant solution, Metals 7 (6) (2017) 222.
[23] P.Z. Xiang, Y.M. Zhang, Q. Liu, Gold leaching from printed circuit board scrap with thiosulfate, IOP Conf. Ser.: Mater. Sci. Eng 394 (2018) 022001.
[24] S. Ubaldini, D. Guglietta, F. Vegliò, V. Giuliano, Valorization of mining waste by application of innovative thiosulphate leaching for gold recovery, Metals 9 (3) (2019) 274.
[25] Y. Lin, X.Z. Hu, F.T. Zi, Y.L. Chen, S.L. Chen, X.R. Li, L. Zhao, Y.F. Li, Synergistical thiourea and thiosulfate leaching gold from a gold concentrate calcine with copper-ammonia catalysis, Sep. Purif. Technol. 327 (2023) 124928.
[26] Y. Zhang, Q. Li, X.L. Liu, T. Jiang, A thermodynamic analysis on thiosulfate leaching of gold under the catalysis of Fe^{3+}/Fe^{2+} complexes, Miner. Eng. 180 (2022) 107511.
[27] Y. Ou, Y.B. Yang, K. Li, W. Gao, L. Wang, Q. Li, T. Jiang, Eco-friendly and low-energy innovative scheme of self-generated thiosulfate by atmospheric oxidation for green gold extraction, J. Clean. Prod 387 (2023) 135818.
[28] Q. Wang, X.Z. Hu, F.T. Zi, P. Yang, Y.L. Chen, S.L. Chen, Environmentally friendly extraction of gold from refractory concentrate using a copper–ethylenediamine–thiosulfate solution, J. Clean. Prod 214 (2019) 860–872.
[29] A. Behnamfard, M.M. Salarirad, F. Veglio, Process development for recovery of copper and precious metals from waste printed circuit boards with emphasize on palladium and gold leaching and precipitation, Waste Manag 33 (11) (2013) 2354–2363.
[30] X.R. Li, L. Zhao, S.L. Chen, Y. Lin, X.Z. Hu, F.T. Zi, Highly efficient and selective extraction of Au(I) from thiosulfate gold-leaching solution using diphenylphosphine, J. Environ. Chem. Eng 12 (1) (2024) 111750.
[31] F. Xie, J.N. Chen, X.Z. Zhang, B. Xu, W. Wang, Adsorption mechanism of copper and gold thiosulfates onto activated carbon, Trans. Nonferrous Met. Soc. China 33 (10) (2023) 3210–3221.
[32] Z.L. Dong, T. Jiang, B. Xu, J.T. Wu, Q. Li, Y.B. Yang, A comparative study of electrodeposition and sodium dithionite reduction for recovering gold in gold-rich solution from the adsorption of thiosulfate solution by ion exchange resin, Sep. Purif. Technol. 328 (2024) 125053.
[33] S. Raiguel, L. Gijsemans, A. Van den Bossche, B. Onghena, K. Binnemans, Solvent extraction of gold(III) with diethyl carbonate, ACS Sustainable Chem. Eng 8 (36) (2020) 13713–13723.
[34] L.L. Zhao, Q.S. Zhou, Y. Yang, Y. Zhang, Y.W. Qiu, Y.J. Chen, X. Jin, X.J. Yang, S.X. Wang, Ultra-high adsorption capacity and selectivity of photo-enhanced sulfur-rich M_2S_3 (M = Bi and Sb) for gold recovery from electronic wastewater, J. Water Process. Eng 57 (2024) 104572.
[35] Y. Xiang, C.Y. Cheng, M.H. Liu, W.C. Bai, Z.X. Zang, L. Xu, Y. Yu, G.J. Liu, Efficient recovery of gold using Macroporous Metal-Organic framework prepared by the 'MOF in MOF' method, Sep. Purif. Technol. 335 (2024) 126131.
[36] Z.L. Dong, T. Jiang, B. Xu, Y.B. Yang, Q. Li, An eco-friendly and efficient process of low potential thiosulfate leaching-resin adsorption recovery for extracting gold from a roasted gold concentrate, J. Clean. Prod 229 (2019) 387–398.
[37] T. Ouchi, S. Wu, T.H. Okabe, Recycling of gold using anodic electrochemical deposition from molten salt electrolyte, J. Electrochem. Soc 167 (12) (2020) 123501.
[38] M. Matsumiya, R. Kinoshita, Y. Sasaki, Recovery of gold by solvent extraction and direct electrodeposition using phosphonium-based ionic liquids, J. Electrochem. Soc 169 (8) (2022) 082513.
[39] D.Y. Hou, F.N. Bai, P. Dong, J. Chen, Y.T. Zhang, F.M. Meng, Z.H. Zhang, C.X. Zhang, Y.J. Zhang, J. Hu, Recent development of low temperature plasma technology for lithium-ion battery materials, J. Power Sources 584 (2023) 233599.
[40] K.G. Sun, M. Tebyetekerwa, C. Wang, X.F. Wang, X.W. Zhang, X.S. Zhao, Electrocapacitive deionization: Mechanisms, electrodes, and cell designs, Adv. Funct. Mater. 33 (18) (2023) 2213578.
[41] M.L. Sall, A.K.D. Diaw, D. Gningue-Sall, A. Chevillot-Biraud, N. Oturan, M. Ali Oturan, J.J. Aaron, Removal of Cr(VI) from aqueous solution using electro-synthesized 4-amino-3-hydroxynaphthalene-1-sulfonic acid doped polypyrrole as adsorbent, Environ. Sci. Pollut. Res. 24 (26) (2017) 21111–21127.
[42] A. Nosal-Wiercińska, M. Martyna, M. Wiśniewska, Influence of mixed 2-thiocytosine–ionic surfactants adsorption layers on kinetics and mechanism of Bi(III) ions electro reduction: use of the nanostructured R-AgLAFE, Appl. Nanosci. 13 (7) (2023) 4737–4745.
[43] Y. Yin, Y. Peng, M. Zhou, P. Zhang, Y. Cheng, P. Chen, X. Xing, X. Ma, Q. Zhu, X. Sun, Q. Qian, X. Kang, B. Han, Highly efficient zinc electrode prepared by electrodeposition in a salt-induced pre-phase separation region solution, Sci. Bull. 68 (20) (2023) 2362–2369.

[44] Z.W. Hu, R.T. Wu, X.M. Pang, C.H. Yu, X.M. Jian, Adsorption of phosphorus in water by metal-modified large-size biochar: Realizing the recovery and recycling of phosphorus, Sustain. Chem. Pharm. 36 (2023) 101279.
[45] Z. Alimohamadi, H. Younesi, N. Bahramifar, Desorption of Reactive Red 198 from activated carbon prepared from walnut shells: effects of temperature, sodium carbonate concentration and organic solvent dose, Adv. Environ. Technol. 2 (3) (2017) 137–141.
[46] A. Mansoor, S. Anjum, Z. Mustafa, R. Khurram, M. Sattar, T. Ilayas, Erbium substituted baddeleyites ($Er_xZr(1-x)O_2$): Structural, ferroelectric, magnetic and electrochemical analysis for supercapacitors electrodes using walnut shells charcoal, Ceram. Int. 49 (24) (2023) 39825–39842.
[47] K.Y. Zhu, J. Ma, J.Z. Cong, T. Zhang, H.J. Lei, H.D. Xu, Z.S. Luo, M. Li, The road to reuse of walnut by-products: a comprehensive review of bioactive compounds, extraction and identification methods, biomedical and industrial applications, Trends Food Sci. Technol 143 (2024) 104264.
[48] L. Lu, R. Shan, Y. Shi, S. Wang, H. Yuan, A novel TiO_2/biochar composite catalysts for photocatalytic degradation of methyl orange, Chemosphere 222 (2019) 391–398.
[49] F. Terzi, N. Dossi, Ti as an electrode material. How to make the future better than the present, Anal. Bioanal. Chem 407 (24) (2015) 7257–7261.
[50] W.Q. Zhan, X. Zhang, Y. Yuan, Q.Z. Weng, S.X. Song, M. de Jesús Martínez-López, J.L. Arauz-Lara, F.F. Jia, Regulating chemisorption and electrosorption activity for efficient uptake of rare earth elements in low concentration on oxygen-doped molybdenum disulfide, ACS Nano 18 (9) (2024) 7298–7310.
[51] A. Zeriouh, L. Belkbir, Thermal decomposition of a Moroccan wood under a nitrogen atmosphere, Thermochim. Acta 258 (1995) 243–248.
[52] R.K. Sharma, J.B. Wooten, V.L. Baliga, X.H. Lin, W.G. Chan, M.R. Hajaligol, Characterization of chars from pyrolysis of lignin, Fuel 83 (11-12) (2004) 1469–1482.
[53] D.Y. Chen, K.H. Cen, X.Z. Zhuang, Z.Y. Gan, J.B. Zhou, Y.M. Zhang, H. Zhang, Insight into biomass pyrolysis mechanism based on cellulose, hemicellulose, and lignin: evolution of volatiles and kinetics, elucidation of reaction pathways, and characterization of gas, biochar and bio-oil, Combust. Flame 242 (2022) 112142.
[54] A.A. Tenimu, Thermogravimetric and dfferential thermal investigation of rice husk cellulose, Bayero J. Pure App. Sci. 12 (1) (2020) 6–11.
[55] Y.B. Tao, S.J. Li, P. Li, Q.L. Wu, Thermogravimetric analyses (TGA) of lignins isolated from the residue of corn stover bioethanol (CSB) production, Holzforschung 70 (12) (2016) 1175–1182.
[56] Y.H. Dou, Q.S. Bai, W.M. Guo, H.F. Wang, S.D. Chen, T.T. Wang, Study on the adsorption characteristics of organic contaminants on alumina surface coated with clean graphene and the influence of amorphous carbon on wetting behavior, Appl. Surf. Sci. 643 (2024) 158658.
[57] K.M. Popov, V.E. Arkhipov, A.G. Kurenya, E.O. Fedorovskaya, K.A. Kovalenko, A.V. Okotrub, L.G. Bulusheva, Supercapacitor performance of binder-free buckypapers from multiwall carbon nanotubes synthesized at different temperatures, Phys. Status Solidi B 253 (12) (2016) 2406–2412.
[58] T. Kesavan, M. Sasidharan, Palm spathe derived N-doped carbon nanosheets as a high performance electrode for Li-ion batteries and supercapacitors, ACS Sustainable Chem. Eng 7 (14) (2019) 12160–12169.
[59] B. Tang, L.P. Zheng, X.C. Dai, H.J. Chen, Nitrogen/oxygen co-doped porous carbons derived from a facilely-synthesized Schiff-base polymer for high-performance supercapacitor, J. Energy Storage 26 (2019) 100961.
[60] Y. Itoh, M.J. Bröcker, S. Sekine, D. Söll, S. Yokoyama, Dimer–dimer interaction of the bacterial selenocysteine synthase SelA promotes functional active-site formation and catalytic specificity, J. Mol. Biol 426 (8) (2014) 1723–1735.
[61] W.Q. Zhan, Y. Yuan, B.Q. Yang, F.F. Jia, S.X. Song, Construction of MoS_2 nano-heterojunction via ZnS doping for enhancing *in situ* photocatalytic reduction of gold thiosulfate complex, Chem. Eng. J. 394 (2020) 124866.
[62] K. Kiyohara, T. Sugino, K. Asaka, Phase transition in porous electrodes, J. Chem. Phys. 134 (15) (2011) 154710.
[63] D.A. Bograchev, A.D. Davydov, Non-steady-state natural convection in a model electrochemical system with vertical and horizontal plane electrodes, Russ. J. Electrochem 39 (9) (2003) 967–972.
[64] H. Yu, F.T. Zi, X.Z. Hu, Y.H. Nie, P.Z. Xiang, J. Xu, H. Chi, Adsorption of the gold–thiosulfate complex ion onto cupric ferrocyanide (CuFC)-impregnated activated carbon in aqueous solutions, Hydrometallurgy 154 (2015) 111–117.
[65] H. Yu, F.T. Zi, X.Z. Hu, Y.H. Nie, Y.L. Chen, H.L. Cheng, Adsorption of gold from thiosulfate solutions with chemically modified activated carbon, Adsorpt. Sci. Technol. 36 (1-2) (2018) 408–428.
[66] Y.L. Chen, F.T. Zi, X.Z. Hu, Y. Lin, H.H. Du, J. Hu, P. Yang, Y. Zhang, B.M. Yang, The first effective utilization of activated carbon in gold thiosulfate system: A more eco-friendly, easier method for gold recovery and material regeneration, Miner. Eng. 155 (2020) 106441.
[67] C.W. Wang, S.L. Chen, Y.L. Chen, F.T. Zi, X.Z. Hu, X.C. Qin, Y. Zhang, P. Yang, Y. He, P.Q. He, Y. Lin, G.F. Zhang, Modification of activated carbon by chemical vapour deposition through thermal decomposition of thiourea for enhanced adsorption of gold thiosulfate complex, Sep. Purif. Technol. 241 (2020) 116632.